The Journal of Green Energy and Environmental Engineering

Research Paper

Study on Mechanical Properties and Microstructure of Lightweight High-Toughness Ultra-High Performance Concrete

Mark Taylor[1], Kerry Ahmad[1], David Eastwood[2,*]

[1] Division of Chemistry of Renewable Resources, Department of Chemistry, University of Natural Resources and Life Sciences, Vienna, Konrad-Lorenz-Str. 24, A-3430 Tulln, Austria
[2] Institut Charles Gerhardt Montpellier, UMR 5253, CNRS- ENSCM-UM - Equipe Ingénierie et Architectures Macromoléculaires, Université Montpellier, CC 1702, Place Eugène Bataillon, 34095 Montpellier Cedex 5, France
*Corresponding author: Eastwood.mas03@univ-montpellier2.fr

Abstract. Lightweight modification of Ultra-High Performance Concrete (UHPC) represents a key pathway for its sustainable development. This study prepared Lightweight UHPC (LUHPC) by synergistically incorporating hollow glass microspheres (HGM) and fly ash cenospheres (FAC) as replacements for cement and quartz sand. The effects of lightweight modification on macroscopic mechanical properties were systematically evaluated by comparing the compressive strength, axial tensile performance, and apparent density of reference and lightweight specimens, complemented by microstructural analysis to reveal the evolution of hydration products and interfacial transition zone characteristics. Incorporating lightweight components successfully reduced the density of LUHPC by 497.2 kg/m³ while retaining a high compressive strength of 146.6 MPa. Although the tensile strength (9.7 MPa) is marginally lower than that of conventional UHPC (11.2 MPa), the material exhibits distinct strain-hardening behavior, demonstrating excellent tensile ductility. In LUHPC, the pozzolanic activity of fly ash cenospheres consumed more $Ca(OH)_2$ during hydration, generating C-S-H gel with a low calcium-to-silicon (Ca/Si) ratio and a higher degree of hydration. Hollow glass microspheres improved particle packing and optimized the interfacial structure. The synergistic effect of these two components yielded a denser matrix microstructure, demonstrating superior strength-density compatibility.

Keywords: *Lightweight Ultra-High-Performance Concrete (LUHPC); Mechanical properties; Microstructure; Hollow glass microspheres (HGM); Fly ash cenospheres (FAC)*

Received on 03 Feb 2026, Accepted on 24 Mar 2023, Published on 11 May 2023

Copyright © 2026 Cristina Tayeh *et al*. licensed to JGEEE. This is an open access article distributed under the terms of the CC BY-NC-SA 4.0, which permits copying, redistributing, remixing, transformation, and building upon the material in any medium so long as the original work is properly cited.

1 Introduction

The building sector ranks among the most materially demanding industries worldwide, accounting for roughly 30% of global raw material extraction and generating approximately 40% of human-induced carbon dioxide discharges [1]. Within this context, cement concrete, the most widely used construction material, faces a critical paradox: while its high density (typically 2,400–2,600 kg/m³) ensures structural robustness, it simultaneously imposes immense dead loads on superstructures, escalates transportation costs, and exacerbates the carbon footprint associated with cement production [2]. Consequently, the pursuit of high-performance concrete that transcends the traditional trade-off between strength and weight has become a central challenge in modern civil engineering. Ultra-High Performance Concrete, developed during the early 1990s, constitutes a transformative advancement in cementitious material engineering. Its formulation relies on optimized granular packing density, minimal water-to-cementitious ratios, and discontinuous steel fiber reinforcement, yielding compressive capacities surpassing 120 MPa alongside superior resistance to environmental deterioration [3–5]. Nevertheless, the substantial self-weight of conventional UHPC restricts its deployment in gravity-sensitive applications—including extended-span bridges, vertical high-rise structures, and modular prefabricated systems—where mass reduction is critical for both economic viability and seismic performance optimization [6].

Lightweight UHPC (LUHPC) has thus emerged as a strategic solution to reconcile the conflict between ultra-high

strength and low density. By incorporating lightweight aggregates (LWAs) to partially or fully replace traditional dense aggregates (like quartz sand) and cementitious binders, LUHPC aims to achieve a density reduction of 20–30% while retaining the mechanical integrity of its parent material [7]. Yet, the introduction of LWAs is a double-edged sword. Conventional LWAs, such as expanded clay or shale, often suffer from high water absorption and rough surface textures, which can compromise the interfacial transition zone (ITZ) and lead to unpredictable mechanical behavior [8]. Therefore, the selection of appropriate lightweight materials and the optimization of their synergistic effects within the UHPC matrix are critical research frontiers.

Current research on LUHPC has predominantly focused on two categories of lightweight materials: porous ceramic aggregates and hollow glass microspheres (HGM). Studies by Lu et al. [9] demonstrated that substituting cement with HGM at volumes up to 50% could reduce density to approximately 1,900 kg/m³ while maintaining compressive strengths above 100 MPa. HGM offer the advantages of low density, smooth surfaces, and minimal water absorption, which facilitate improved flowability and reduced bleeding. However, their inert nature and weak bonding with the cement matrix often result in brittle failure and limited tensile ductility [10]. Conversely, fly ash cenospheres (FAC)—hollow spherical particles recovered from coal fly ash—possess not only low density but also latent pozzolanic reactivity. Research indicates that FAC can participate in secondary hydration reactions, consuming calcium hydroxide ($Ca(OH)_2$) to form additional Calcium-Silicate-Hydrate (C-S-H) gel, thereby refining the pore structure [11]. Despite these benefits, FAC often have thinner shells and lower crushing strengths compared to quartz sand, raising concerns about their ability to bear load under high stress [12].

A critical review of existing literature reveals a significant gap: while individual studies have explored HGM or FAC separately, few have systematically investigated the synergistic potential of combining these two distinct lightweight components. The challenge lies in balancing the physical filling effect of HGM with the chemical reactivity of FAC. Furthermore, most existing studies prioritize compressive strength and density as the sole metrics of success. There is a paucity of data regarding the tensile behavior of LUHPC, particularly its strain-hardening characteristics and cracking resistance, which are vital for structural applications involving dynamic or seismic loads. Additionally, the micro-mechanisms governing the interfacial bonding between multi-scale lightweight aggregates and the UHPC matrix remain insufficiently understood, particularly concerning the Calcium-to-Silicon (Ca/Si) ratio of the C-S-H gel within the ITZ [13].

To circumvent these constraints, the present investigation introduces an innovative hybrid approach integrating Hollow Glass Microspheres and Fly Ash Cenospheres within a UHPC binder matrix. The primary objectives are threefold: Macroscopic Performance Optimization: To systematically evaluate the effect of HGM (replacing cement) and FAC (replacing quartz sand) on the workability, density, compressive strength, and axial tensile properties of LUHPC. Particular emphasis is placed on tensile strain-hardening response, a defining characteristic of advanced fiber-reinforced cementitious materials. Microstructural Mechanism Investigation: Advanced analytical methodologies—including Scanning Electron Microscopy, Energy Dispersive Spectroscopy, Backscattered Electron imaging, and Nanoindentation—were deployed to examine hydration phase assemblages, interfacial transition zone architecture, and micromechanical descriptors (hardness and elastic modulus) within the composite binder matrix. Synergistic Effect Quantification: To elucidate how the physical filling of HGM and the pozzolanic activity of FAC interact to influence the hydration kinetics and microstructural densification, thereby explaining the observed macro-mechanical performance.

2. Raw Materials and Experimental Design

2.1 Raw Materials

The cementitious materials included PII 62.5 cement, silica fume (SF), and fly ash (FA). Fly ash cenospheres (FAC) were used to partially replace quartz sand (QS): FACI (d50= 182.2 μm), FACII(d50= 129.6 μm), and FACIII(d50= 77.2 μm); QSI(d50= 397.2 μm), QSII(d50 = 194.8 μm), and QSIII(d50= 85.3 μm). Tap water, a polycarboxylate-based high-performance water reducer, and 16 mm long brass-plated hooked-end steel fibers were used. The main chemical compositions of the materials are listed in Table 1, and the material properties are shown in Figure 1.

Table 1 Main chemical compositions of the raw material (wt%)

Cementitious materials	SiO_2	CaO	Al_2O_3	Fe_2O_3	MgO	Na_2O	SO_3
Cement	19.69	61.35	5.30	3.55	1.54	0.62	3.12
SF	89.43	0.21	0.29	0.12	0.44	0.23	0.30
HGM	64.65	7.92	0.29	0.07	0.39	7.61	0.35
FA	46.47	8.36	23.06	6.00	1.78	1.17	1.27
FAC	52.44	0.72	33.42	2.38	0.48	0.82	0.38

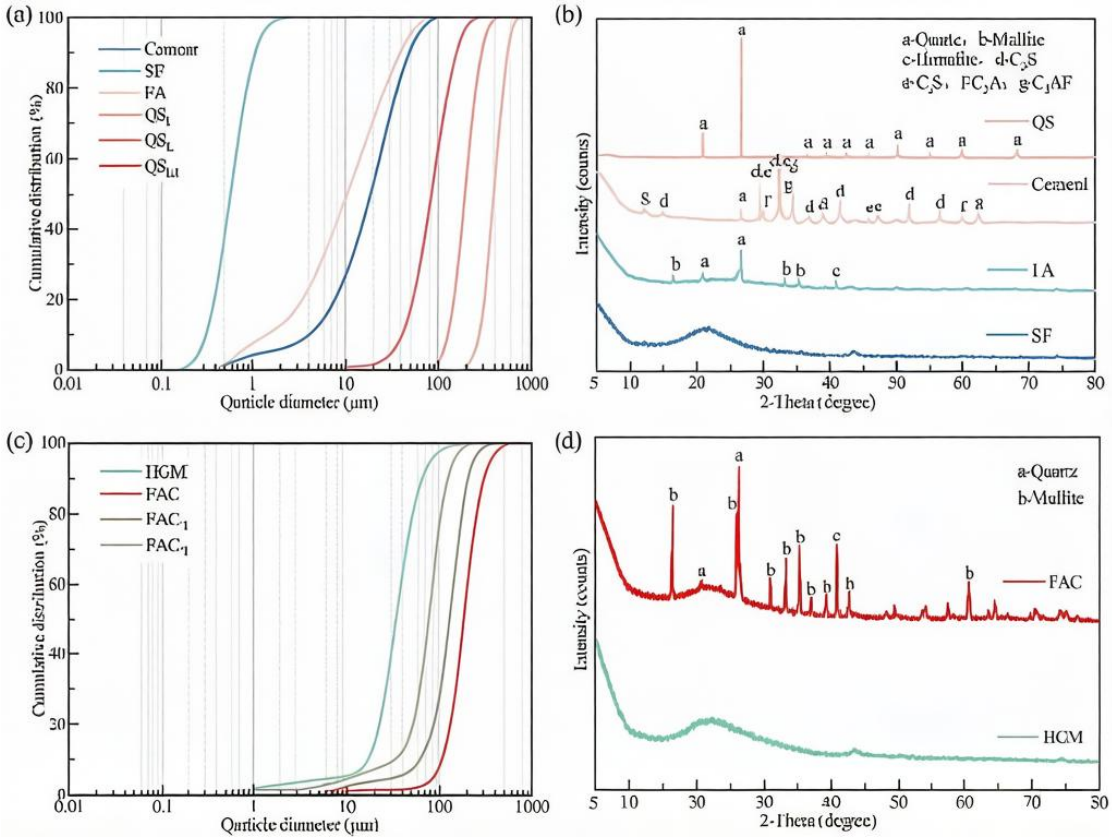

Figure 1 Cumulative particle-size distributions and XRD patterns: (a) Cumulative particle-size distribution of raw materials; (b) XRD pattern of raw materials; (c) Cumulative particle-size distribution of lightweight materials; (d) XRD pattern of lightweight materials.

2.2 Mix Proportions

A UHPC group was set as the reference group. In the LUHPC group, HGM was used to volumetrically replace 50% of the cement to introduce lightweight components while retaining sufficient cementitious activity to maintain the matrix skeleton strength. Simultaneously, ensuring a constant water-binder ratio (0.18), FAC was used to volumetrically replace 55% of the quartz sand. This aimed to satisfy self-compacting performance while utilizing the ball-bearing effect of cenospheres to improve rheological properties. The specific mix proportions are detailed in Table 2.

Table 2 Mix proportions of LUHPC (kg/m³)

Mix No.	Cement	SF	FA	HGM	QS I / FAC I	QS II / FAC II	QS III / FAC III	Water	Superplasticizer	Fiber
UHPC	750	275	125	0	348.3 / 0	348.3 / 0	348.3 / 0	207.0	23	156
LUHPC	375	275	125	71.4	156.7 / 47.0	156.7 / 47.0	156.7 / 47.0	152.4	23	156

2.3 Specimen Preparation

Solid constituents were gravimetrically proportioned and subjected to low-shear blending for 3 min. Aqueous phase was subsequently introduced, followed by high-shear agitation for 5–10 min. Discontinuous steel fibers were then gradually incorporated under continued high-speed mixing for an additional 2 min. The fresh composite was cast into formwork, consolidated via vibration, sealed with polymeric film, and maintained under ambient conditions for 24 h prior to form removal. Accelerated strength development was achieved through 72 h steam conditioning, with subsequent standard moist curing until the 7-day testing interval.

2.4 Mechanical Property Testing

Compressive behavior was evaluated per GB/T 17671-2021 [27] on a 2000 kN servo-hydraulic frame at 2.4 kN/s displacement rate. Test geometries comprised 70.7 mm cubes, 50 mm cubes, and 40 mm × 40 mm × 160 mm prismatic specimens.

Flexural Strength: Tested according to GB/T 17671-2021 [27] using 40 mm × 40 mm × 160 mm specimens at a loading rate of 50 N/s until failure.

Tensile Test: Uniaxial tensile tests were conducted according to JC/T 2461-2018 [28] using a 50 kN electronic universal testing machine in displacement-controlled mode at a rate of 0.3 mm/min.

Apparent Density: Tested according to BS EN 12390-7:2019 [29] using 40 mm × 40 mm × 160 mm samples. Samples were air-dried, weighed, and volume was measured via water displacement to calculate apparent density.

2.5 Microscopic Analysis

2.5.1 Scanning Electron Microscopy (SEM) - Energy Dispersive Spectroscopy (EDS) - Backscattered Electron (BSE) Analysis

The microstructural architecture of LUHPC was examined via Field Emission Scanning Electron Microscopy. EDS was used for qualitative and quantitative micro-area elemental analysis, and BSE was used for microstructural observation.

2.5.2 Nanoindentation

Nanoindentation tests were performed on the fiber-matrix ITZ and aggregate-matrix ITZ to measure the relative distribution of hardness and elastic modulus.

2.5.3 X-ray Diffraction (XRD)

XRD analysis was performed using a D8 ADVANCE X-ray diffractometer. Samples were scanned from 5° to 80° (2θ) at a rate of 10°/min.

3. Results and Analysis

3.1 Mechanical Properties

3.1.1 Compressive Strength and Density

Compressive strength outcomes are presented in Figure 2. Reference UHPC specimens achieved mean compressive capacities of 202.2, 220.7, and 252.2 MPa across varying geometries. Lightweight UHPC counterparts registered 107.0, 122.4, and 146.6 MPa, respectively, manifesting pronounced dimensional dependency [30]. The mean strength of the LUHPC group was approximately 100 MPa lower than that of the UHPC group. This reduction is attributed to the replacement of approximately 50% of the cement and quartz sand with HGM and FAC, which increased the number of pores in the matrix, and the lower crushing value of FAC, which reduced matrix strength.

The apparent density of the specimens was measured according to section 1.4.4. The actual apparent density of the LUHPC group specimens was 1872.6 kg/m³, significantly lower than the 2369.8 kg/m³ of the UHPC group. Despite the incorporation of lightweight constituents diminishing LUHPC mechanical capacity, the concurrent mass reduction proved substantially more pronounced, yielding a specific strength index (compressive capacity normalized by bulk density) averaging 78.3 kN·m/kg—a performance benefit especially accentuated within ultra-high strength regimes [31].

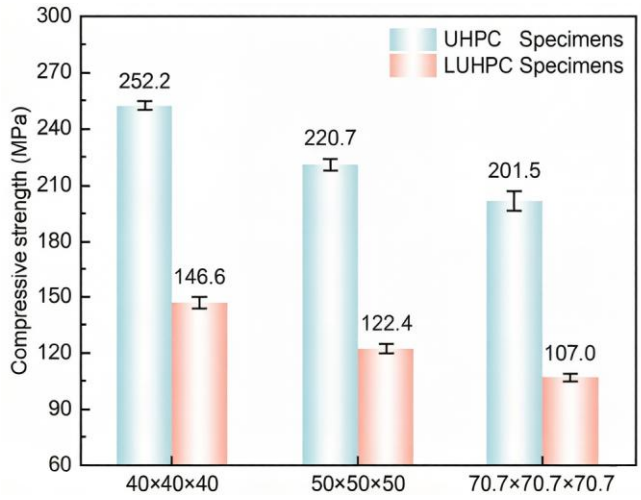

Figure 2 Compressive strength of specimens.

3.1.2 Flexural Strength

Flexural capacity outcomes are summarized in Table 3. Mean flexural strengths for the two cohorts were 41.6 MPa and 40.9 MPa, respectively.

Table 3 Flexural strength of LUHPC

Mix No.	Specimen dimensions (mm³)	Specimen 1 (MPa)	Specimen 2 (MPa)	Specimen 3 (MPa)	Mean (MPa)
UHPC		43.4	41.9	39.6	41.6
LUHPC	40 × 40 × 160	44.3	42.5	36.0	40.9

The lightweight UHPC formulation exhibited marginally inferior flexural performance relative to the conventional UHPC reference. This phenomenon is mainly attributed to the substitution of raw materials by lightweight materials and the change in fly ash content within the system. The introduction of lightweight materials reduced the compactness of the UHPC matrix. After a large amount of cement was replaced, the proportion of fly ash in the entire system increased, and the incorporation of FAC reduced hydration products to some extent, leading to a decline in matrix strength and toughness. These factors acted together, causing the flexural strength of the LUHPC group to be slightly lower than that of the UHPC group.

3.1.3 Tensile Strength

Uniaxial tension testing was conducted on dog-bone geometries, with Digital Image Correlation employed to

characterize fracture kinematics (Figures 3 and 4). Direct tension capacity registered 11.2 MPa for conventional UHPC and 9.7 MPa for the lightweight variant.

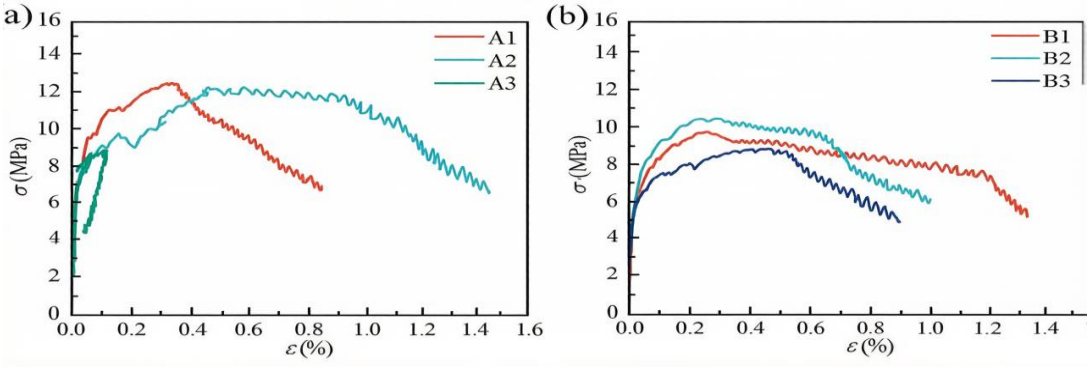

Figure 3 Direct tension test results: (a) Tensile strength of UHPC group; (b) Tensile strength of LUHPC group.

Although a decrease was observed, the reduction rate was low. Combined with DIC analysis, both groups formed multiple micro-cracks during the tensile process, reflecting typical strain-hardening characteristics. However, the strain field distribution in the UHPC specimens was relatively uniform, and the crack propagation paths were relatively straight. In contrast, the strain concentration areas in the LUHPC specimens were more distinct, and the crack propagation paths exhibited a more tortuous morphology. This is because the introduction of low-strength lightweight components resulted in an interfacial transition zone (ITZ) that was weaker compared to traditional aggregates. Micro-cracks tended to initiate and deflect at these weak interfaces [32], which somewhat weakened the overall continuity of the matrix, leading to a slight decrease in the tensile strength of LUHPC. However, it remained at a high level, and the specimens still exhibited significant strain-hardening phenomena during tension, demonstrating excellent deformability and toughness.

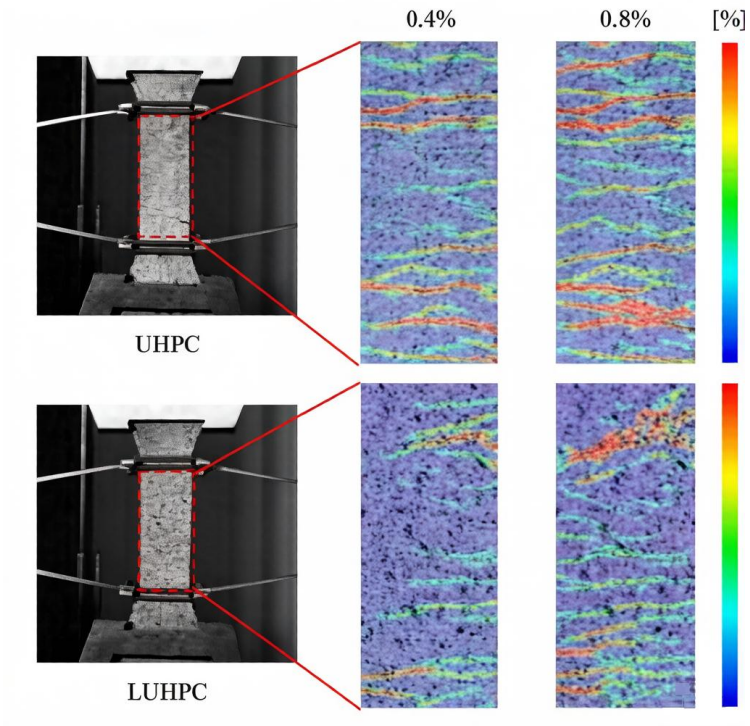

Figure 4 Failure mode under direct tension.

3.2 Microstructure and Mechanism

3.2.1 SEM

The SEM micrographs of the UHPC and LUHPC groups are shown in Figures 5 and 6. In Figure 5(a), the bright, irregular region represents the steel fiber, surrounded by the matrix. A pronounced interfacial void is evident at the steel fiber-matrix boundary, with the reinforcement surface exhibiting minimal surface roughness. The inadequate mechanical anchorage between fiber and cementitious matrix yields compromised interfacial adhesion. In Figure 5(b), angular crystalline particulates correspond to quartz sand inclusions, which demonstrate intimate matrix integration absent of visible microfractures, corroborating the elevated compressive capacity of the reference UHPC formulation. Figure 6(a) similarly reveals discernible interfacial cracking at the steel fiber-matrix transition within the lightweight UHPC system. Additionally, numerous gray-black pores are distributed on the matrix surface, confirming that the compactness of the LUHPC group is reduced. In Figure 6(b), the ellipsoidal shapes are FAC, which are tightly bonded to the matrix interface. However, since they are hollow spheres, they are more susceptible to crushing under load, which also contributes to the decrease in macroscopic compressive strength of LUHPC.

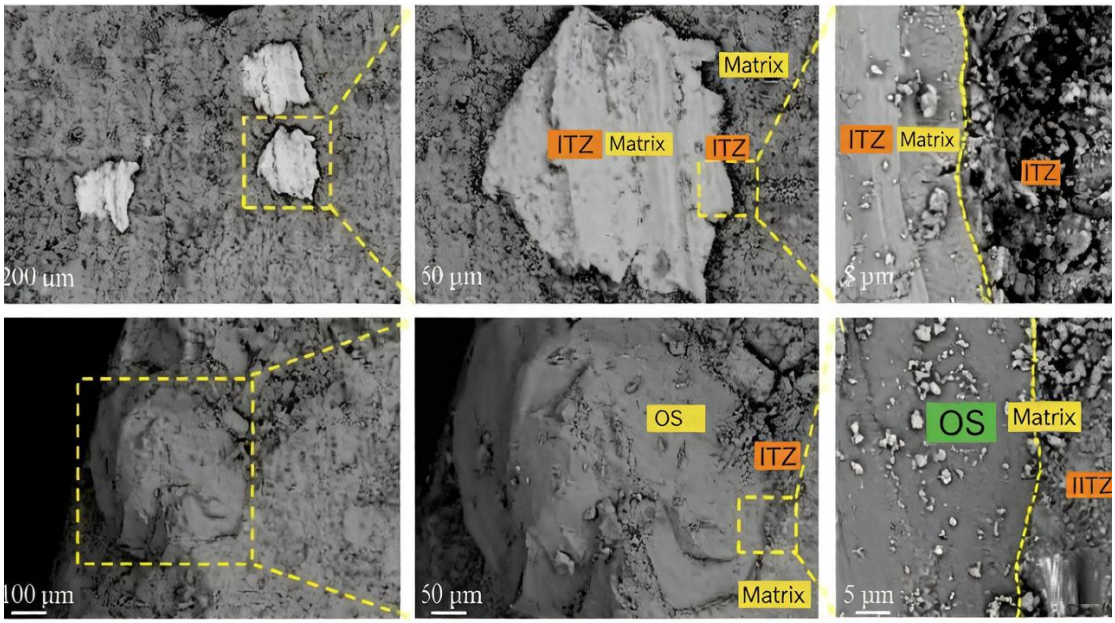

Figure 5 Microstructure of the UHPC group: (a) Steel fiber, matrix, and their ITZ; (b) Quartz sand, matrix, and their ITZ.

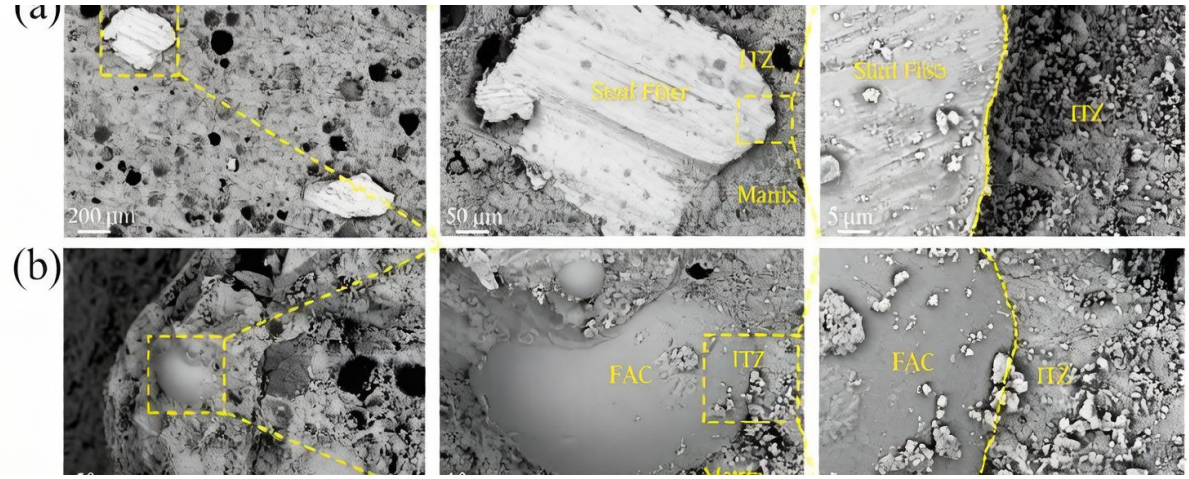

Figure 6 Microstructure of the LUHPC group: (a) Steel fiber, matrix, and their ITZ; (b) Fly-ash

cenosphere, matrix, and their ITZ.

3.2.2 BSE

Backscattered electron micrographs for both formulations are presented in Figure 7. Comparative examination of Figures 7(a) and 7(b) reveals substantial incorporation of low-grayscale porosity and lightweight filler particulates within the LUHPC binder matrix. This is because cement and quartz sand were largely replaced in LUHPC, and the proportion of fly ash increased relatively, leading to a reduction in hydration products and further decreasing the compactness of the matrix.

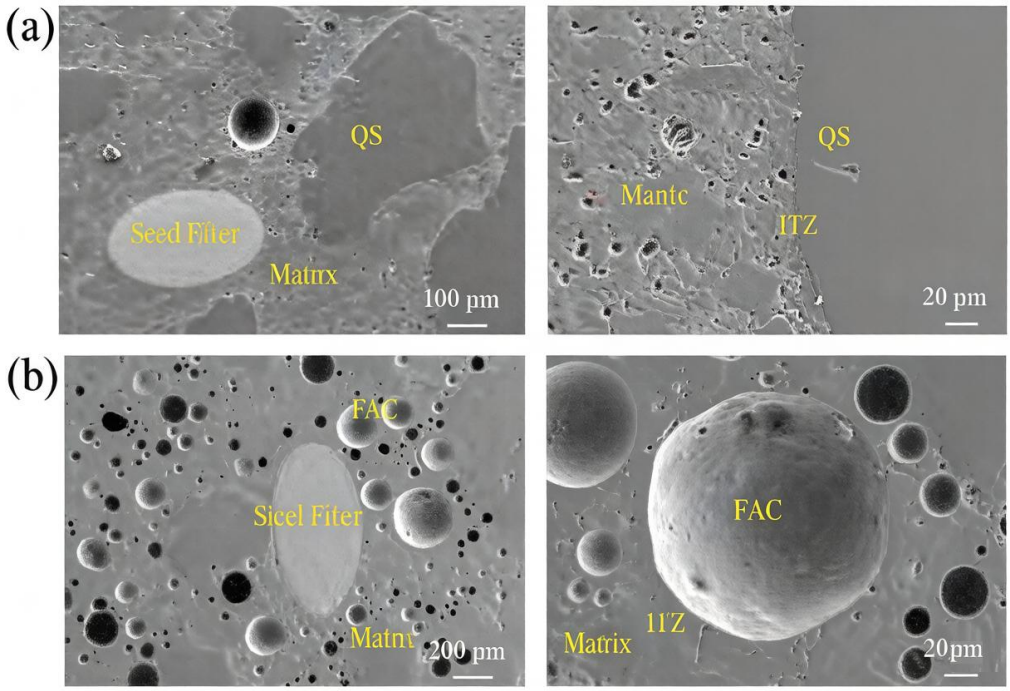

Figure 7 Microstructure: (a) UHPC group; (b) LUHPC group.

3.2.3 EDS

EDS surface scanning and point scanning were used to quantitatively analyze the hydration products and degree of the two groups, with results shown in Figures 8 and 9 (green markers in the figures indicate selected point scanning areas). Surface scanning results in Figure 8 indicate that the Ca/Si ratios of the UHPC and LUHPC groups were 0.54 and 0.38, respectively. In the UHPC system, Ca/Si mainly reflects the compositional characteristics of hydration products (e.g., C-S-H gel). The lower Ca/Si in the LUHPC group is attributed to the incorporation of HGM (main component SiO_2) and FAC (main components Al_2O_3 and SiO_2), which reduced the overall Ca content in the system while increasing the content of reactive SiO_2, thereby lowering the Ca/Si ratio.

Studies indicate that the ITZ width between fine aggregates and cement paste in UHPC systems is typically around 20 μm [33]. In the LUHPC group, fine aggregates were partially replaced by FAC, whose main components include reactive Al_2O_3 and SiO_2. Under hydrothermal curing regimes, the external shell of fly ash cenospheres engages in pozzolanic activity, progressively depleting portlandite to precipitate calcium-silicate-hydrate gel characterized by diminished Ca/Si stoichiometry. Tobermoritic phases with suppressed calcium content exhibit superior nanomechanical attributes, extending the mean silicate chain length and polymeric condensation degree of C-S-H [33], consequently expanding the interfacial transition zone breadth. Simultaneously, high temperatures promote the dissolution of SiO_2 from silica fume, increasing the silicon content in the gel and further reducing Ca/Si. However, due to the high number of pores, although the ITZ showed improvement, the overall mechanical properties were still affected.

EDS point analyses presented in Figure 9 further demonstrate suppressed Ca/Si ratios at both the steel fiber-

matrix and aggregate-matrix interfacial transition zones within the LUHPC formulation relative to the UHPC reference. The pozzolanic reactivity of fly ash cenospheres facilitated accelerated secondary hydration under steam curing conditions [34]. Compared to chemically inert quartz sand, FAC exhibited diminished surface Ca/Si values, corroborating the elemental mapping observations.

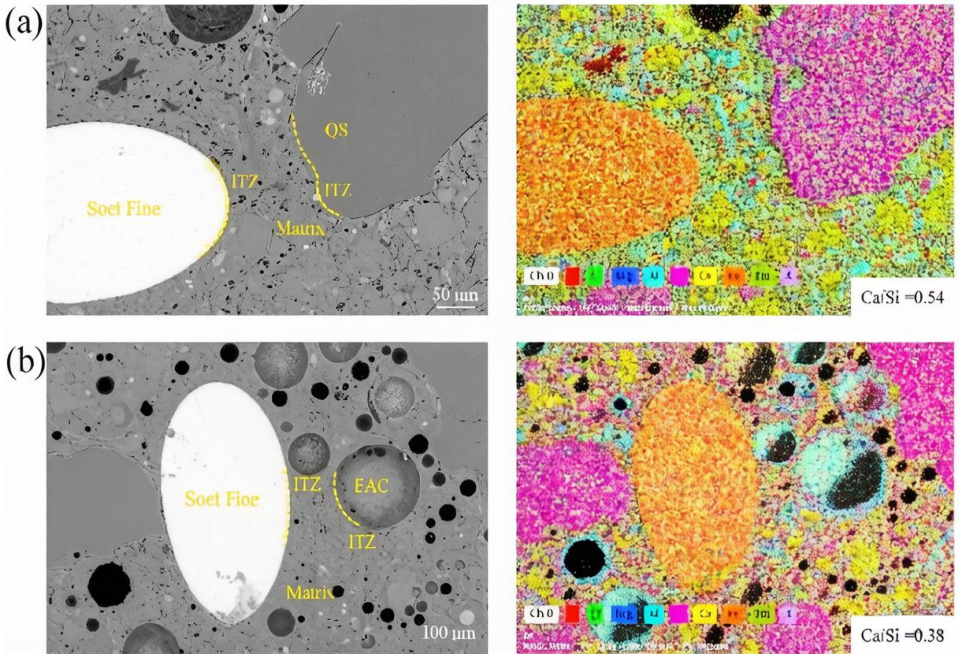

Figure 8 Ca/Si analysis of hydration products: (a) Surface scan results of the UHPC group; (b) Surface scan results of the LUHPC group.

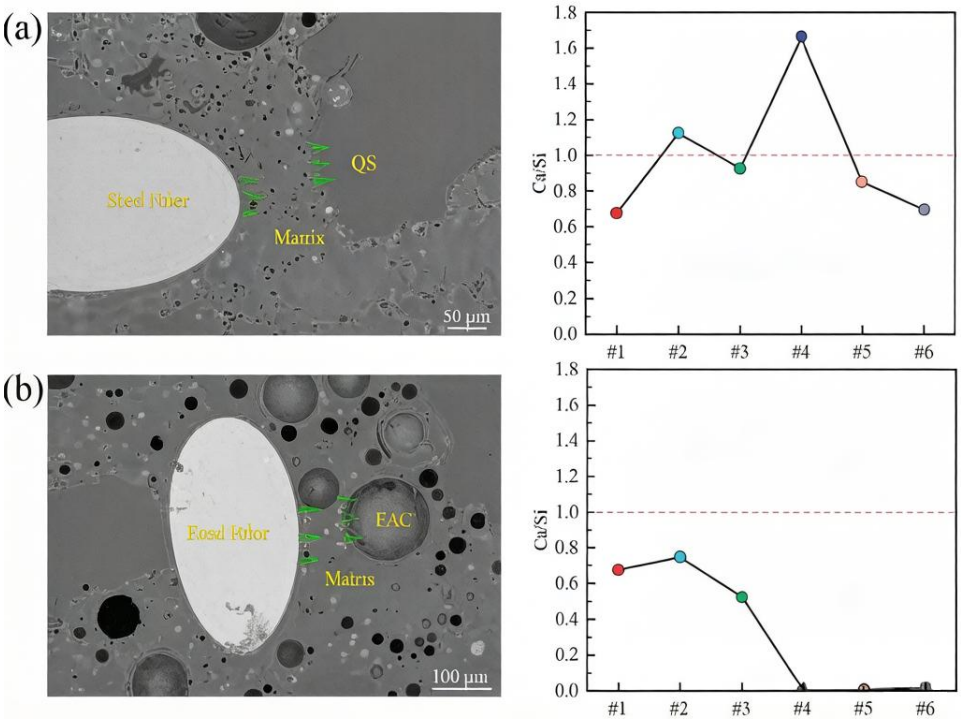

Figure 9 Ca/Si analysis of the interfacial transition zone: (a) Selected area and point-scan results of the UHPC group; (b) Selected area and point-scan results of the LUHPC group.

3.2.4 Nanoindentation and XRD

Nanoindentation was ultimately employed to quantitatively characterize the micromechanical behavior of steel fibers, cementitious matrix, aggregate inclusions, and their corresponding interfacial transition zones. Representative force-displacement curves are depicted in Figure 10. The steel reinforcement registered the maximum peak indentation force, succeeded by quartz sand particulates, whereas fly ash cenospheres demonstrated the minimal peak load resistance. Steel fibers, being metallic materials, possess high hardness and elastic modulus, corresponding to the high peak load. Quartz sand, primarily composed of silica (SiO_2), has high hardness but moderate elastic modulus, with its secondary high peak load determined by its high hardness but brittle characteristics. Fly ash cenospheres are mainly composed of amorphous Al_2O_3-SiO_2 glass, have low hardness, small elastic modulus, and a hollow structure, corresponding to the low peak load.

The nanoindentation locations and corresponding hardness and elastic modulus results are shown in Figure 11. Analysis shows that the elastic modulus of steel fibers was the largest (140–200 GPa), with a hardness of 7–11 GPa. Quartz sand was next (60–100 GPa and 8–12 GPa), and FAC was the lowest (20–40 GPa and 0–2 GPa). This is consistent with the peak load results. Additionally, it was found that the hardness and elastic modulus of the FAC-matrix ITZ were higher than those of the quartz sand-matrix ITZ. This is because low Ca/Si C-S-H has a higher degree of polymerization and a denser structure, resulting in significantly higher hardness and elastic modulus compared to high Ca/Si C-S-H.

X-ray diffraction was conducted to identify crystalline hydration phases in both formulations. As illustrated in Figure 12, the dominant mineralogical constituents in the reference UHPC system comprised quartz (SiO_2), calcite ($CaCO_3$), calcium-silicate-hydrate gel, alite (C_3S), and belite (C_2S). No distinct diffraction peaks for calcium hydroxide ($Ca(OH)_2$) were found, likely because secondary hydration reactions of silica fume and fly ash consumed a large amount of $Ca(OH)_2$ under steam curing conditions. Additionally, diffraction peaks for AFm phases were observed around 12°, resulting from the reaction of carbonates in the system with monocarbonate hydration products to form AFm. Significantly, the quartz diffraction peak intensity in the lightweight UHPC formulation was substantially attenuated relative to the reference group, attributable to extensive quartz sand substitution by fly ash cenospheres. Moreover, C-S-H peak intensity was considerably diminished in the LUHPC system. As the predominant binding phase in cementitious matrices, C-S-H abundance and structural ordering govern mechanical performance. The observed C-S-H depletion in LUHPC stems primarily from reduced Portland cement content necessitated by lightweight filler incorporation, consequently limiting hydrate precipitation. Moreover, around 16°, a diffraction peak for gehlenite appeared in the LUHPC group. This is because fly ash and fly ash cenospheres provided Al_2O_3 and SiO_2, which reacted with $Ca(OH)_2$ in cement under alkaline high-temperature conditions to form gehlenite, further consuming $Ca(OH)_2$ in the system. This product exerts a complex influence on the material's microstructure and mechanical properties.

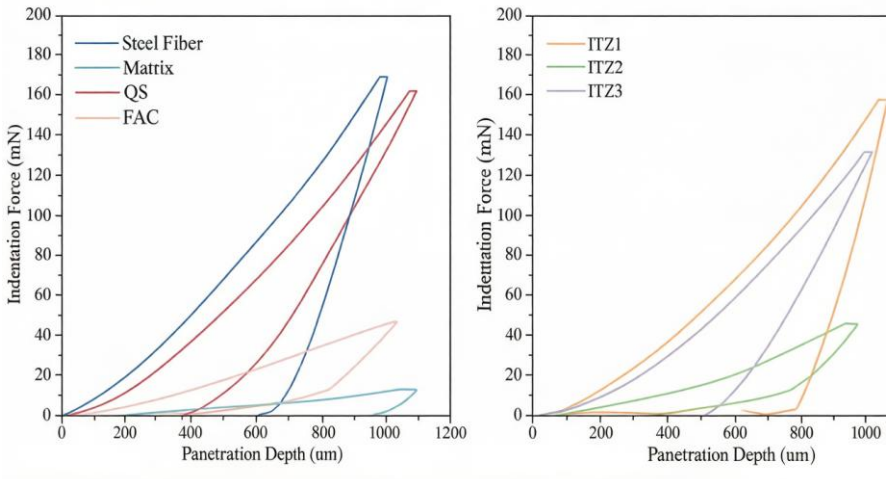

Figure 10 Typical load-penetration depth curve from nanoindentation (ITZ1: steel fiber-matrix ITZ; ITZ2: quartz sand-matrix ITZ; ITZ3: fly-ash cenosphere-matrix ITZ).

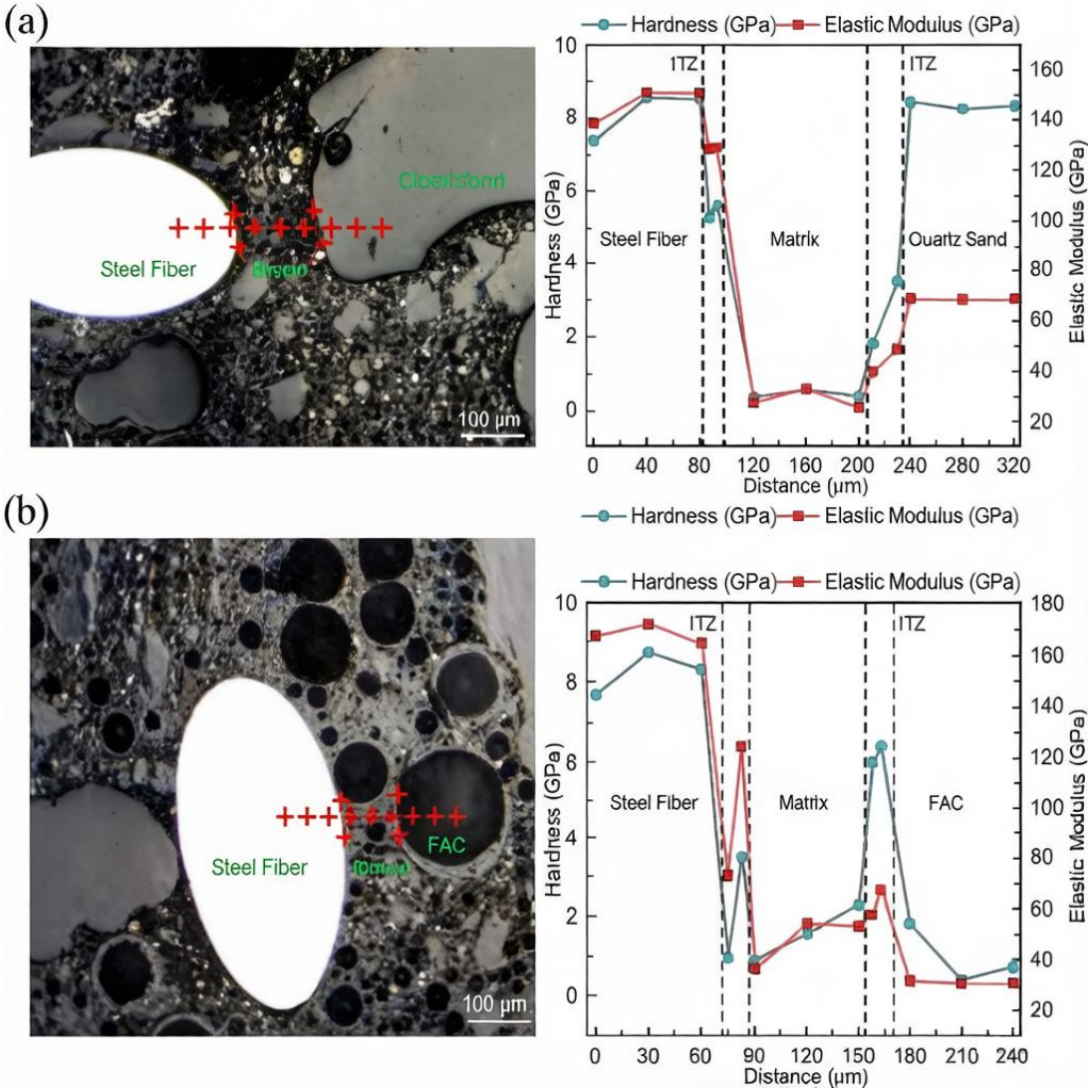

Figure 11 Nanoindentation points and corresponding hardness and elastic modulus results: (a) UHPC group; (b) LUHPC group.

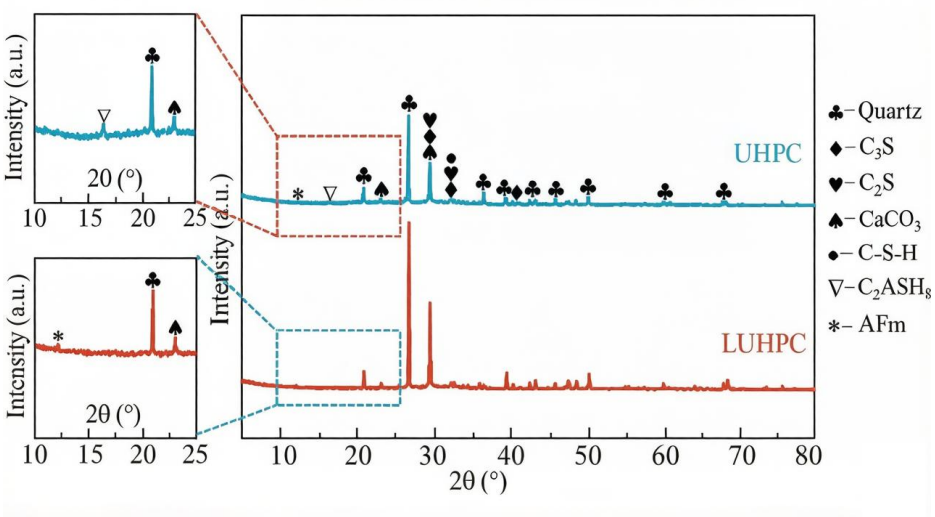

Figure 12 XRD test results.

This study advances the design philosophy of lightweight ultra-high-performance concrete (LUHPC) by demonstrating that the synergistic integration of hollow glass microspheres (HGM) and fly ash cenospheres (FAC) can effectively reconcile the traditionally conflicting demands of low density, high strength, and tensile ductility. By replacing 50% of cement with HGM and 55% of quartz sand with FAC, the composite achieves a density reduction of 497.2 kg/m³—representing a ~21% decrease relative to conventional UHPC—while retaining a compressive strength of 146.6 MPa. Although this strength is lower than that of the reference UHPC (252.2 MPa), the material exhibits a specific strength of 78.3 kN·m/kg, underscoring the efficiency of the lightweight design. Crucially, the tensile performance remains robust: LUHPC retains 9.7 MPa tensile strength (only ~13% lower than conventional UHPC) and displays pronounced strain-hardening behavior accompanied by multiple micro-cracking, as revealed by Digital Image Correlation. This ductility is particularly valuable for structural resilience under dynamic or seismic loading, where energy absorption and crack control are paramount. The preservation of tensile toughness despite strength reduction is attributed to the combined physical and chemical effects of the lightweight fillers: HGM improve particle packing and reduce matrix stiffness discontinuities, while FAC contribute pozzolanic reactivity that enhances interfacial bonding and refines the pore structure. These findings challenge the conventional assumption that lightweight modification inevitably compromises mechanical integrity, offering instead a pathway to optimize performance-density trade-offs in high-performance cementitious systems.

Microstructural analysis provides a mechanistic explanation for the observed macroscale behavior, revealing that the dual-lightweight strategy induces profound changes in hydration chemistry and interfacial architecture. EDS results show that the Ca/Si ratio of C–S–H gel in LUHPC decreases from 0.54 to 0.38, driven by the silica-rich nature of HGM and the aluminosilicate composition of FAC, which dilute calcium availability while increasing reactive SiO_2 content. Under steam curing, the pozzolanic activity of FAC consumes $Ca(OH)_2$ to form low-Ca/Si C–S–H with higher polymerization and denser nanostructure, as confirmed by nanoindentation results showing higher hardness and elastic modulus in the FAC–matrix interfacial transition zone (ITZ) compared to the quartz sand–matrix ITZ. Paradoxically, while the ITZ is chemically strengthened, the overall matrix compactness is reduced due to the lower crushing resistance of FAC and the increased porosity from lightweight inclusions, as evidenced by SEM and BSE imaging. XRD further identifies the formation of gehlenite in LUHPC, a product of the reaction between FAC-derived Al_2O_3 and $Ca(OH)_2$, which contributes to microstructural densification but also reflects the altered hydration pathway. These microstructural insights clarify why LUHPC exhibits slightly reduced compressive strength yet retains excellent tensile ductility: the chemically refined ITZ enhances crack deflection and energy dissipation, while the physical voids introduced by lightweight aggregates act as stress concentrators that limit load transfer. Together, these results establish a nuanced understanding of how multi-scale interactions between physical filler geometry and chemical reactivity govern the performance of lightweight UHPC, providing a foundation for future optimization of mix designs aimed at balancing sustainability, structural efficiency, and mechanical resilience.

4. Conclusion

This paper used Ultra-High Performance Concrete (UHPC) as a control group and prepared Lightweight UHPC (LUHPC) by partially substituting cement and aggregates with hollow glass microspheres and fly ash cenospheres (FAC). The macroscopic mechanical consequences of density-reduction modifications were systematically assessed, with governing mechanisms elucidated through microstructural evolution analysis. The conclusions are as follows:

Although the lightweight materials themselves possess low density and strength, their introduction reduced the apparent density of LUHPC while significantly lowering cement and quartz sand content. This negatively impacted the mechanical properties to some extent but fully utilized material efficiency. In terms of axial tensile performance, compared to UHPC (11.2 MPa), LUHPC retained a high tensile strength (9.7 MPa) while exhibiting distinct strain-hardening phenomena, indicating good toughness.

Distinct cracks existed at the interface between steel fibers and the matrix, whereas quartz sand and FAC were tightly bonded to the matrix. The introduction of FAC resulted in a wider interfacial transition zone (ITZ) between aggregates and the matrix, leading to more pores in the matrix. However, the Ca/Si ratio of this ITZ was lower

than that of the quartz sand-matrix ITZ, and its hardness and elastic modulus were higher, indicating a denser LUHPC microstructure.

The incorporation of low-density, low-strength constituents resulted in a macroscopic compressive capacity of 146.6 MPa for the lightweight UHPC, representing a reduction from the 252.2 MPa achieved by the conventional UHPC reference. However, its density decreased significantly (from 2369.8 kg/m³ to 1872.6 kg/m³), and microscopic hardness and elastic modulus remained high. Furthermore, due to the pozzolanic activity of FAC under steam curing conditions, secondary hydration was promoted to a certain extent, resulting in a higher degree of hydration. Compared to UHPC containing inert aggregates, LUHPC exhibited a lower Ca/Si ratio.

References

[1] TAHWIA A M, ELGENDY G M, AMIN M. Mechanical properties of affordable and sustainable ultra-high-performance concrete[J]. Case Studies in Construction Materials, 2022, 16: e01069.

[2] WEN Decheng, WEI Dingbang, WU Laidi, et al. Research on Mix Design and Characteristics of UHPC Matrix Mixture Based on MAA Model[J]. Journal of Building Materials, 2022, 25(07): 693-699.

[3] ZHANG Yiming, REN Xiaodan, ZHAO Xin. Uniaxial Tensile Viscoplastic Damage Constitutive Model of Ultra-high Performance Concrete[J]. Journal of Building Materials, 2025, 28(11): 1053-1061.

[4] BAHMANI H, MOSTOFINEJAD D. Microstructure of ultra-high-performance concrete(UHPC)-a review study[J]. Journal of Building Engineering, 2022, 50: 104118.

[5] SU X, REN Z, LI P. Review on physical and chemical activation strategies for ultra-high performance concrete(UHPC)[J]. Cement and Concrete Composites, 2024, 149: 105519.

[6] ESMAEILI J, ROMOUZI V, KASAEI J, et al. An investigation of durability and the mechanical properties of ultra-high performance concrete(UHPC) modified with economical graphene oxide nano-sheets[J]. Journal of Building Engineering, 2023, 80: 107908.

[7] LI Lijian, LIU Sumei, XU Fanding, et al. Uniaxial Tensile Behavior of Ultra-high Performance Concrete Containing Coarse Aggregate[J]. Journal of Building Materials, 2024, 27(02): 167-173.

[8] TAHWIA A M, ELGENDY G M, AMIN M. Durability and microstructure of eco-efficient ultra-high-performance concrete[J]. Construction and Building Materials, 2021, 303: 124491.

[9] LU J X. Recent advances in high strength lightweight concrete: From development strategies to practical applications[J]. Construction and Building Materials, 2023, 400: 132905.

[10] LU J X, SHEN P, ZHENG H, et al. Development and characteristics of ultra high-performance lightweight cementitious composites(UHP-LCCs)[J]. Cement and Concrete Research, 2021, 145: 106462.

[11] LU J X, SHEN P, ALI H A, et al. Development of high performance lightweight concrete using ultra high performance cementitious composite and different lightweight aggregates[J]. Cement and Concrete Composites, 2021, 124: 104277.

[12] ZHANG H, LIANG Q, SHAO M, et al. Optimization of low-carbon lightweight foamed concrete using ground circulating fluidized bed fly ash[J]. Journal of Cleaner Production, 2025, 489: 144697.

[13] DAHAL M, LIYEW G, KIM H K, et al. Characteristics of ultra-high performance lightweight concrete containing hollow glass microspheres under severe loading conditions[J]. Construction and Building Materials, 2022, 356: 129312.

[14] LU J X, SHEN P, SUN Y, et al. Strategy for preventing explosive spalling and enhancing material efficiency of lightweight ultra high-performance concrete[J]. Cement and Concrete Research, 2022, 158: 106842.

[15] PAN H, YAN S, ZHAO Q, et al. Preparation and properties of ultra-high performance lightweight concrete[J]. Magazine of Concrete Research, 2023, 75(6): 310-323.

[16] ASLANI F, WANG L, ZHENG M. The effect of carbon nanofibers on fresh and mechanical properties of lightweight engineered cementitious composite using hollow glass microspheres[J]. Journal of Composite Materials, 2023, 53(17): 2447-2464.

[17] AHN J, MOON J, PAE J, et al. Microplastics as lightweight aggregates for ultra-high performance concrete: Mechanical properties and autoignition at elevated temperatures[J]. Composite Structures, 2023, 321: 117333.

[18] MENG L, DING Y, LI L, et al. Study on dynamic properties of lightweight ultra-high performance concrete(L-UHPC)[J]. Construction and Building Materials, 2023, 399: 132526.

[19] LU J X, SHEN P, ALI H A, et al. Mix design and performance of lightweight ultra high-performance concrete[J].

Materials & Design, 2022, 216: 110553.
[20] ABADEL A A. Physical, mechanical, and microstructure characteristics of ultra-high-performance concrete containing lightweight aggregates[J]. Materials, 2023, 16(13): 4883.
[21] GUO K, DING Q. Effect of shale powder on the performance of lightweight ultra-high-performance concrete[J]. Materials, 2022, 15(20): 7225.
[22] XIE Y, ZHOU Q, LONG G, et al. Experimental investigation on mechanical property and microstructure of ultra-high-performance concrete with ceramsite sand[J]. Structural Concrete, 2022, 23(4): 2391-2404.
[23] GUO P, MENG W, DU J, et al. Lightweight ultra-high-performance concrete(UHPC) with expanded glass aggregate: Development, characterization, and life-cycle assessment[J]. Construction and Building Materials, 2023, 371: 130441.
[24] WANG Long, CHI Yin, XU Lihua, et al. Size Effect of Mechanical Properties of Hybrid Fiber Ultra-high Performance Concrete[J]. Journal of Building Materials, 2022, 25(08): 781-788.
[25] HOU D, ZHANG X, ZHANG K, et al. Optimizing lightweight UHPC through the synergy of lightweight aggregate, filler, and polymer fiber via response surface methodology[J]. Construction and Building Materials, 2025, 463: 140104.
[26] ZHANG Y X, ZHANG Q, XU L Y, et al. Transfer learning for intelligent design of lightweight Strain-Hardening Ultra-High-Performance Concrete(SH-UHPC)[J]. Automation in Construction, 2025, 175: 106241.
[27] State Administration for Market Regulation. Method of testing cements—Determination of strength (ISO method): GB/T 17671-2021[S]. Beijing: Standards Press of China, 2021.
[28] Ministry of Industry and Information Technology of the People's Republic of China. Test methods for mechanical properties of high ductility fiber reinforced cementitious composites: JC/T 2461-2018[S]. Beijing: China Building Materials Industry Press, 2018.
[29] Testing hardened concrete—Part 7: Density of hardened concrete: BS EN 12390-7:2019[S]. British Standards Institution, 2019.
[30] SHUI Liangliang. Size effect on compressive strength and shrinkage characteristics of ultra-high performance concrete[J]. Journal of Building Materials, 2019, 22(4): 632-637.
[31] Standard Practice for Fabricating and Testing Specimens of Ultra-high Performance Concrete: ASTM C1856/C1856M[S]. American Society of Testing Materials, 2017.
[32] ZHANG Gensheng, LIU Genjin, GUO Xingnan, et al. Experimental Study on Force-Electricity Coupling of Steel Fiber Reinforced Concrete after Cracking[J]. Journal of Inner Mongolia University of Technology (Natural Science Edition), 2025, 44(03): 261-266.
[33] ZHANG H, JI T, ZENG X, et al. Mechanical behavior of ultra-high performance concrete(UHPC) using recycled fine aggregate cured under different conditions and the mechanism based on integrated microstructural parameters[J]. Construction and Building Materials, 2018, 192: 489-507.
[34] CHEN Meng, FENG Jun, ZHANG Tong. Dynamic Splitting Tensile Behavior of Ultra-High Performance Concrete after Exposition to Elevated Temperature[J]. Journal of Building Materials, 2025, 28(02): 118-126.